Journal of Catalysis 404 (2021) 67–79

Contents lists available at ScienceDirect

Journal of Catalysis

journal homepage: www.elsevier.com/locate/jcat

A study of the mechanism of triglyceride hydrodeoxygenation over alumina-supported and phosphatized-alumina-supported Pd catalysts

Anna Vikár [a], Hanna E. Solt [a], Gyula Novodárszki [a], Magdolna R. Mihályi [a], Róbert Barthos [a], Attila Domján [b], Jenő Hancsók [c], József Valyon [a], Ferenc Lónyi [a,*]

[a] Institute of Materials and Environmental Chemistry, Research Centre for Natural Sciences, Magyar tudósok körútja 2, 1117 Budapest, Hungary
[b] Centre for Structural Science, Research Centre for Natural Sciences, Magyar tudósok körútja 2, 1117 Budapest, Hungary
[c] Research Centre for Biochemical, Environmental and Chemical Engineering, Department of MOL Hydrocarbon and Coal Processing, University of Pannonia, Veszprém, 8200 Veszprém, Hungary

ARTICLE INFO

Article history:
Received 14 June 2021
Revised 24 August 2021
Accepted 31 August 2021
Available online 8 September 2021

Keywords:
Hydrodeoxygenation
Pd/γ–Al_2O_3
Pd/phosphatized γ–Al_2O_3
Tricaprylin
Valeric acid

ABSTRACT

The mechanism of catalytic hydrodeoxygenation (HDO) of fats, vegetable oils, and fatty acids was studied using alumina-supported Pd catalysts and tricaprylin and valeric acid as model reactants. The chemistry of fatty acid/catalyst interaction was studied by quasi-operando Diffuse Reflectance Infrared Fourier Transform Spectroscopy (DRIFTS). The Pd/γ–Al_2O_3 catalyst showed good activity in the hydrogenolysis reaction of the ester bonds to convert tricaprylin to caprylic acid, but they were of poor activity in the consecutive hydrodeoxygenation (HDO) of the acid to paraffin. The surface modification of the support alumina by phosphate groups significantly increased the HDO activity of the Pd catalyst and, consequently, the paraffin yield. The activity change was accounted partly for the partial replacement of the weak base Al–OH groups by weak acid P–OH groups but mainly for the partial elimination of Lewis acid ($Al^{\oplus}$) – Lewis base ($O^{\ominus}$) pair sites on the surface of the support. Both surface Al–OH and P–OH groups were shown to participate in the reaction with carboxylic acid and formed bidentate surface carboxylate species, which further reacted with hydrogen to give paraffin. Carboxylates of less basic surface sites were found to be more prone to HDO reaction than those of strong base sites. Monodentate carboxylates, formed on $Al^{\oplus}$ $O^{\ominus}$ pair sites were of low reactivity. Phosphatizing eliminated most of the Lewis type acid-base pair sites, therefore, reactive bidentate carboxylates represented the most abundant surface intermediate (MASI) during the HDO reaction of triglyceride. The hydroxyl coverage of the carboxylated surface was shown to become somewhat higher under steady-state reaction conditions. The increased hydroxyl coverage implies that C–O bond hydrogenolysis of the surface carboxylate proceeds, regenerating OH groups and forming aldehyde that could be intermediate of paraffin formation.

1. Introduction

The extensive combustion of fossil carbon is most probably responsible for the growing concentration of greenhouse gas CO_2 in the atmosphere. The concerns about global warming turned attention towards the production of biofuels by upgrading non-edible and waste vegetable oils and animal fats [1–8]. The most widely used production method of diesel range bio-oil, generally referred to as biodiesel, is catalytic transesterification of latter renewable triglycerides by lower alcohols [1,6,7]. However, the biodiesel cannot fully replace conventional diesel oil, because of its lower energy density, higher viscosity, moderate oxidation stability, and limited compatibility with fossil fuel [4,6]. A better alternative of triglyceride upgrading is deoxygenation via hydroprocessing that is providing a mixture of hydrocarbons. The hydrocarbon mixture is second generation biofuel, often referred to as biogasoil or green diesel. Biogasoil has comparable or even better fuel properties than conventional diesel fuel [6,7,9].

Catalytic triglyceride HDO can be carried out at moderate temperature (200 – 400 °C) and hydrogen pressure (<50 bar). The applied catalysts are those, routinely used in the petroleum industry for hydroprocessing, such as, sulfided cobalt and nickel molybdate catalysts, supported noble (Pt, Pd, Ru) and non-noble metals (Ni, Cu, Co), metal phosphides, metal oxides, etc. [3,4,6,10]. Application of monometallic transition metal catalysts are very common for the deoxygenation of fatty acids and triglycerides [3,6,10]. Palladium based catalysts are especially preferred because of the

* Corresponding author.
E-mail address: lonyi.ferenc@ttk.hu (F. Lónyi).

https://doi.org/10.1016/j.jcat.2021.08.052
0021-9517/

peculiar ability of the palladium metal to activate hydrogen for reaction [10]. Nevertheless, there is a general agreement that the catalyst support does not only provide high surface area to stabilize high metal dispersion, but it also has significant contribution to the HDO activity and selectivity by its acid-base property [4,6,10]. Supports, having strong Brønsted acidity, such as H-zeolites, are less favored because they initiate cracking of long chain paraffins and condensation reactions, producing coke precursors and coke that deactivates the catalyst [6,10]. Therefore, supports of mild-to-moderate acidity, such as activated carbon, TiO_2, ZrO_2, SiO_2, and Al_2O_3 were found suitable for HDO catalysts [4,6,10]. The most often used support is γ–Al_2O_3 [4,8].

The hydroconversion of triglycerides to paraffins proceeds in the consecutive steps of ester bond hydrogenolysis, giving carboxylic acid, and deoxygenation of the acid to paraffin. The deoxygenation reaction is the rate determining step of paraffin formation [3,4,6,11]. Former studies showed that the deoxygenation reaction of the carboxylic acid intermediate over Pd catalysts follows pathways resulting in the formation of CO (hydrodecarbonylation, HDCO), CO_2 (hydrodecarboxylation, HDCO2), and H_2O (H_2-reduction of oxygen, HDH2O). Over supported metal catalysts the HDCO was found to be the major reaction route, whereas the HDCO2 and HDH2O were reaction routes, which had only minor contribution to the HDO reaction [7,8]. The mechanisms of these HDO pathways are not fully understood. It was suggested that the HDCO reaction proceeded through direct hydrogenolysis of the carboxylic acid to paraffin and formic acid (C–C bond scission), which reaction step was followed by quick decomposition of HCOOH to CO and H_2O [6,8,11]. Deoxygenation on the HDH2O route was proposed to proceed by deoxygenation of carboxylic acid to aldehyde intermediate [2,3,5,8]. Accordingly, formation of aldehyde from carboxylic acid involves hydrogenation/dehydration reactions (hydrogenation of C = O bond to CH–OH followed by H_2O formation involving C–O bond scission). The surface-bound aldehyde intermediate is then further hydrogenated to paraffins by releasing either H_2O or CO, corresponding to routes HDH2O and HDCO, respectively [3,5].

In the present study, alumina-supported Pd catalysts were prepared and studied to learn more about the mechanism of triglyceride HDO reaction. The effect of support phosphatization on the catalyst structure, acid-base properties, and activity was investigated. The HDO activity was tested using tricaprylin and valeric acid model compounds. Quasi–operando DRIFTS investigation provided insight in the chemistry of surface intermediate formation during the catalytic reaction and permitted to come to important conclusions, concerning some mechanistic details.

2. Experimental

2.1. Catalyst preparation

Alumina-supported palladium catalyst was perepared by impregnating 10 gramms of γ–Al_2O_3 (Ketjen CK-300, Alfa Aesar) by 10 cm^3 of aqueous $Pd(NH_3)_4(NO_3)_2$ (product of Strem) solution. The concentration of the solution was adjusted to get catalyst of 0.5 wt% Pd content. The sample was dried at 110 °C for 16 h. To decompose the metal precursor salt the sample was calcined. It was heated first at a heating rate of 2 °C min^{-1} to 150 °C, kept at this temperature for 1 h, and then the temparature was raised at a heating rate of 4 °C min^{-1} to 350 °C. The catalyst was kept at this tempreture for additional 4 h. The obtained catalyst sample was designated as Pd/Al_2O_3.

The phosphatized-alumina-supported Pd catalyst samples were prepared following the same procedure as above, except that the alumina support was phosphatized first to different extents. Supports with 1.0, 2.5, and 5.0 wt% phosphorous content were prepared by impregnating 10 g of γ–Al_2O_3 with 10 cm^3 of a solution, containing calculated amount of phosphoric acid. The impregnated samples were dried at 110 °C for 16 h then calcined in air at 550 °C for 4 h to generate the phosphatized alumina supports. The thus obtained phosphatized γ–Al_2O_3 catalyst supports are designated as Al_2O_3–1P, Al_2O_3–2.5P and Al_2O_3–5P, respectively. These supports were used to prepare catalysts of 0.5 wt% Pd content. The corresponding supported Pd catalysts were designated as Pd/Al_2O_3–1P, Pd/Al_2O_3–2.5P, and Pd/Al_2O_3–5P.

2.2. Catalyst characterization

2.2.1. Elemental analysis

The P and Pd content of the catalyst samples were determined by using Inductively Coupled Plasma Optical Emission Spectroscopic (ICP-OES) method (Spectro Genesis ICP-OES apparatus).

2.2.2. Specific surface area (SSA)

Nitrogen adsorption isotherms of the catalyst samples were determined at −196 °C using an automatic, volumetric adsorption analyzer (The "Surfer", product of Thermo-Fisher Scientific). The sample was dehydrated before the measurement at 250 °C under high vacuum (10^{-6} mbar) for 4 h. The SSA of the catalyst samples was determined by the BET method, whereas the pore-size distribution was calculated using the Barett-Joyner-Halenda (BJH) method.

2.2.3. X-ray powder diffraction (XRPD)

The XRPD measurements were carried out using a Philips PW 1810/3710 X-ray powder diffractometer in a Bragg-Brentano parafocusing arrangement applying monochromated Cu K_α (λ = 1.5418 A) radiation.

2.2.4. Metal dispersion

The dispersion of Pd in the catalysts was determined by CO pulse chemisorption method. About 100 mg of the sample was placed into a quartz microreactor (I.D.: 4 mm) and reduced in situ in hydrogen flow at 450 °C for 1 h. It was flushed then by He flow at 450 °C for 30 min and cooled to room temperature in the He flow. In 3 min intervals carbon monoxide pulses of 10 μL volume were injected sequentially into the He flow, passing through the catalyst bed. The CO concentration of the reactor effluent was monitored using thermal conductivity detector (TCD). The TCD signal was processed by computer. The introduction of CO pulses was continued until the chemisorption sites were saturated. After calibration the molar amount of chemisorbed CO was calculated from the areas of the TCD signals.

2.2.5. Temperature-programmed CO_2 desorption (CO_2-TPD)

The CO_2-TPD measurement was used to characterize the basicity of the supports. About 150 mg of the sample was placed into a quartz microreactor (I.D.: 4 mm) and activated in O_2-flow at 550 °C for 1 h. The sample was then flushed with N_2 for 15 min at 550 °C, evacuated at the same temperature for 30 min and cooled to room temperature. Adsorption of CO_2 was carried out by contacting the sample with CO_2 gas at 13.3 kPa for 15 min. The system was flushed by He and the temperature of the reactor was ramped up at a rate of 10 °C min^{-1} to 700 °C. The CO_2 concentration in the gas flow was monitored by TCD.

2.2.6. Fourier Transform Infrared spectroscopy (FT-IR)

A Nicolet 6700 FT-IR (Thermo Scientific) instrument was used in transmission mode to record the spectra of the surface species present on the neat supports and catalysts and obtained from adsorption of compounds. Self-supporting wafer of the examined sample

having a "thickness" of 5–10 mg cm^{-2} was placed into the sample holder of a stainless steel spectroscopic cell equipped with CaF_2 windows and a furnace section for in situ activation of the sample either in atmospheric gas flow or under high vacuum. Spectra were taken by averaging 512 scans at a nominal resolution of 2 cm^{-1}.

The acidity and basicity of the supports were studied by determining the spectra of adsorbed pyridine (Py) or CO_2, respectively. Prior to Py adsorption the sample was pretreated at 450 °C under high vacuum (10^{-6} mbar) for 1 h then the temperature was lowered to 200 °C and the sample was contacted with Py vapor at 5 mbar for 30 min. The sample was cooled then to 100 °C. The Py vapor was removed from the cell by successive evacuation at temperatures 100, 200, 300, 400, and 450 °C for 30 min at each temperature. After each evacuation a spectrum was recorded at room temperature. The spectrum of the wafer, recorded before Py adsorption, was subtracted from each spectrum to obtain the spectrum of the adsorbed species only.

A procedure, similar to that described above, was followed to determine the spectra of the species obtained from adsorption of CO_2. Wafer of the activated sample was contacted with CO_2 at 15 mbar at room temperature for 30 min. The spectrum of the adsorbed species from CO_2 was measured after successive evacuation at room temperature, 100, 200, 300, and 400 °C under high vacuum for 30 min at each temperature.

The electronic state of Pd in the catalysts was characterized by analyzing the FTIR spectrum of adsorbed species formed from CO. Prior to CO adsorption, the Pd-containing catalyst wafer was reduced at 450 °C in H_2 stream for 1 h. The catalyst was contacted with CO gas at 5 mbar at room temperature for 20 min then the spectrum of the carbonyl species formed was recorded after 20 min evacuation under high vacuum at room temperature. Each absorbance spectra were scaled to 5 mg cm^{-2} wafer thickness to allow quantitative comparisons.

2.2.7. Magic angle spinning solid-state nuclear magnetic resonance (MAS NMR)

Spectra were recorded using a Varian NMR System spectrometer operating at 600 MHz ^1H frequency (242.74 MHz for ^{31}P and 156.26 MHz for ^{27}Al) with a Chemagnetics 3.2 mm narrow-bore triple resonance T3 probe in double resonance mode. The ^{31}P direct polarization spectra were recorded (160 transients) at 20 °C with 12 kHz of spinning rate and 300 s repetition delay. The ^{27}Al – ^1H cross polarization spectra were recorded (12000 transients) with 0.5 ms contact time, 5 s of repetition delay at 20 °C with 12 kHz of spinning rate. For both experiments SPINAL ^1H decoupling was used. As chemical shift reference ammonium dihydrogen phosphate (δ_{iso} = 0.81 ppm with respect to 85 wt% H_3PO_4 solution) for the ^{31}P and sodium aluminate (δ_{iso} = 79.3 ppm) for the ^{27}Al measurements was used.

2.2.8. Catalytic experiments

Hydroconversion of tricaprylin was investigated using a high pressure fixed-bed flow-through microreactor system. The catalytic reactor (I.D.: 8 mm) was filled with 2.0 g of catalyst using its 0.315–0.630 mm sieve fraction. Prior to the catalytic run, the catalyst was reduced in situ in 50 $cm^3\,min^{-1}$ flow of H_2 at 450 °C for 2 h at atmospheric pressure, then the temperature was lowered to the desired reaction temperature (300 or 350 °C) and the pressure was increased to 21 bar total pressure. The tricaprylin reactant was fed into the reactor using a high-pressure syringe pump (ISCO) at a weight hourly space velocity (WHSV) of $4 g_{tricaprylin} g^{-1}_{catalyst} h^{-1}$, whereas the H_2/tricaprylin molar ratio was 20. The product mixture was cooled to room temperature and the liquid products were separated from the gas products in a reflux condenser downstream of the reactor. The effluent gas leaving the condenser through a back pressure regulator valve contained mainly H_2, and CO (as main product), CO_2, and minor amount of CH_4. The effluent was analysed on-line using a gas chromatograph (GC) equipped with a TCD detector and a 60/80 Carbonex-1000 (L 15.0 ft × OD 1/8″) stainless steel column. The liquid product from the presurized collection vessel was first transferred into a closed atmospheric vessel. During this transfer, the pressure of the vessel reached the system pressure, which was then released via a transfer line connected to a syringe, where the gas, expanded to atmospheric pressure, was collected. Note that this latter expanded gas contained all of those products, which were in liquid phase under system pressure but appeared as gases at atmospheric pressure (mainly propene, and some ethane in H_2). The liquid sample, drained now from atmospheric pressure, was analyzed by GC equipped with flame ionization detector (FID) using CP-FFAP CB (L 25.0 m × ID 0.32 mm × df 0.3 μm) capillary column, whereas the expanded gas products were analysed by GC-TCD-FID using ShinCarbon ST (L 2.0 m × ID 1/8 in. × OD 2.0 mm) column. Samples were taken in every hour after the steady state was reached (after one hour time of stream). At high tricaprylin conversions, when the reactant was converted almost completely into paraffins, the liquid product split into two clear, colorless hydrocarbon and water phases. Since the lower aqueous phase contained only a negligible amount of organic components, in such cases only the composition of the upper organic phase was analyzed. In some cases, when the tricaprylin conversion was not complete, and/or was not completely converted into paraffins, a single phase liquid product was obtained, which was analysed for the organic components. In some cases, when unknown components were also formed, GC–MS equiped with Rxi-5Sil MS (L 30.0 m × ID 0.25 mm × df 0.25 μm) column was used for peak assignments.

2.2.9. Diffuse reflectance Infrared Fourier Transform spectroscopy (DRIFTS)

Quasi-operando DRIFT spectroscopic investigation of the adsorbed species formed from carboxylic acid intermediate under catalytic conditions is crucial in order to reveal structure–activity relationships of the catalyst in the HDO reaction of triglycerides or fatty acids. The experiments were carried out using an FT-IR spectrometer (Thermo Nicolet iS10) equipped with a Collector II diffuse reflectance mirror system and a flow-through DRIFT spectroscopic reactor cell (I.D.: 5 mm, height of catalyst bed ∼ 4 mm) filled with about 20 mg of powdered catalyst sample. The design of the cell allows carrier gas or gas phase reactant mixture to flow through the catalyst bed in the sample cup. The reactant is introduced into the cell by switching the carrier gas flow to a gas saturator containing the reactant at room temperature. Due to the experimental difficulties related to the very low vapor pressure of caprylic acid, valeric acid (VA) was used as model compound in these experiments. First, the catalyst was pre-treated in situ in a 50 $cm^3\,min^{-1}$ H_2 flow at 450 °C for 2 h and then the spectrum of the activated catalyst powder was collected (512 scans at a nominal resolution of 2 cm^{-1}) at the desired reaction temperatures (300 or 350 °C). The reaction of VA was initiated by switching the H_2 or He flow (50 $cm^3\,min^{-1}$) to the gas saturator. The thus obtained H_2/VA or He/VA mixture contained 258 ppm VA. The spectrum taken in the presence of the reacting gas mixture at 300 or 350 °C was corrected with the spectrum of the pure catalyst at the same temperature. Since the contribution of the gas phase spectrum was found negligible under the applied conditions, the thus obtained difference spectrum practically reflects the bands of surface species formed (positive bands) or consumed (negative bands) in the VA adsorption/reaction process.

The effluent gas leaving the reactor cell was continuously monitored by online mass spectrometer (MS; VG ProLab, Thermo Scien-

tific) following the characteristic masses of the major reaction products: butane (m/z = 58, $C_4H_{10}^+$), pentane (m/z = 72, $C_5H_{12}^+$), CO (m/z = 28, CO^+), and CO_2 (m/z = 44, CO_2^+). All signals were corrected for the contribution of other reaction products giving a fragment at the same m/z value.

3. Results

3.1. Catalyst composition and structure

The measured Pd and P contents of the catalysts, listed in Table 1, are in good agreement with the values that follow from the applied conditions of catalyst preparation.

The nitrogen adsorption isotherms, shown in Fig. S1, are characteristic for mesoporous oxides. They are classified as type IV isoterms, having H2 type hysteresis loop. The SSA of the catalysts decreased as their phosphorous content was increased (Table 1). The SSA of the Pd/Al_2O_3–5P catalyst is about 40 % lower than that of the Pd/Al_2O_3 catalyst. These results suggest that phosphate groups can block some pores of the alumina support and thereby decrease the SSA.

XRPD patterns of the phosphatized catalysts and that of the parent γ–Al_2O_3 support are shown in Fig. 1. The diffractograms of the support and all the catalysts were similar, i.e., no new crystalline phase could be detected (Fig. 1). The results suggest that the size of the Pd or PdO particles on the support is well below the detection limit of the XRPD method (the diameter was less than about 5 nm).

The Pd dispersion (D_{Pd}) was obtained as the ratio of the number of surface Pd atoms and the total number of Pd atoms in the catalyst. The molar amount of chemisorbed CO was taken to be equivalent with half of the molar amount of surface Pd atoms [12].

Assuming spherical particle shape and that the three low-index planes are in equal proportions on the polycrystalline surface of the face-centered cubic crystals of the metal, the mean Pd particle size (d_{Pd}) was calculated from the dispersion by the equation

$$d_{Pd} = 6\frac{v}{aD_{Pd}} \quad (1)$$

where v is the volume occupied by a single Pd atom in the bulk of metal ($1.47{\cdot}10^{-2}$ nm^3), and a is the average surface area occupied by one Pd atom ($7.93{\cdot}10^{-2}$ nm^2) [13]. The Pd dispersions and the mean particle sizes, listed in Table 1, barely changed with the phosphorous content of the catalysts.

3.2. Surface properties of the catalysts

3.2.1. Surface hydroxyls

The FT-IR spectra measured for the phosphate-free and phosphatized γ–Al_2O_3 supports in the range of stretching vibration of surface OH groups are shown in Fig. 2. The assignment of the alumina OH bands, first given by Knözinger and Ratnasamy [14], was later refined by Busca et al. [15–17]. The ν_{OH} bands above about 3700 cm^{-1} were assigned to terminal OH groups. The band at 3792 cm^{-1}, appearing as a weak shoulder in the spectrum of pure γ–Al_2O_3 (Fig. 2a) was attributed to ν_{OH} vibration of groups linked to tetrahedral aluminum ions. The band at 3773 cm^{-1} belongs to OH groups next to a coordinately unsaturated tetrahedral aluminum atom, i.e. next to a Lewis acid site. In a very recent paper [18] the assignment of the band at about 3780–3770 cm^{-1} was made more accurate. The band was shown to stem from hydroxyl groups bound to octahedrally coordinated surface Al^{3+} ions (O_5-Al^{VI}-OH sites) that transforms to pentacoordinated Al^{3+} surface sites ("bare" O_5Al^V sites) upon thermal dehydroxylation.

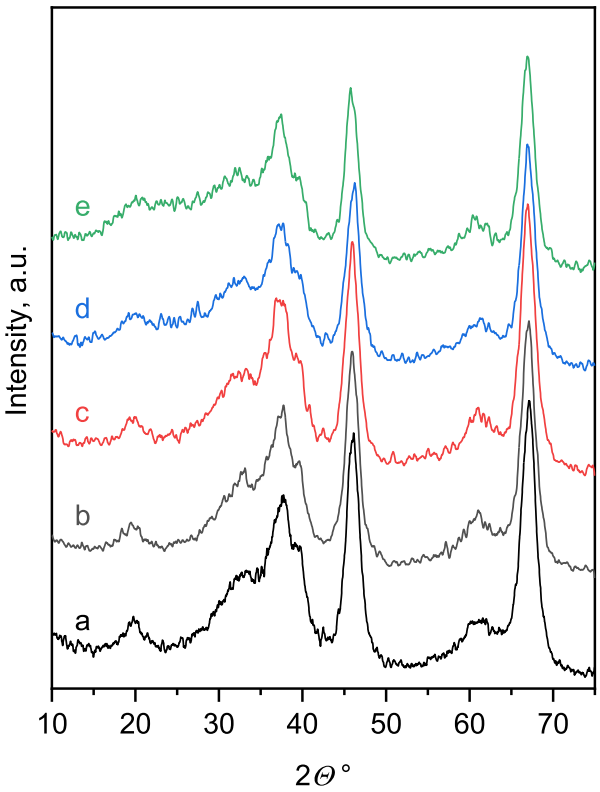

Fig. 1. XRPD patterns of (a) parent γ–Al_2O_3, and (b) Pd/Al_2O_3, (c) Pd/Al_2O_3–1P, (d) Pd/Al_2O_3–2.5P, and (e) Pd/Al_2O_3–5P catalyst samples.

The relatively broad band, centered at 3730 cm^{-1} (Fig. 2a) was assigned to OH groups bound to octahedrally coordinated Al^{3+} ions [15–17]. The presence of a coordinately unsaturated octahedral aluminum atom adjacent to an OH group, results in OH band, shifted to the 3740–3700 cm^{-1} frequency region [15–17]. However, we could not distinguish these bands because of the band broadening and strong overlapping (Fig. 2a). The OH bands below about 3700 cm^{-1} are attributed to different bridging OH species [15–17]. Thus, the broad band centered approximately at 3670 cm^{-1} can be assigned to bridging OH species, whereas the

Table 1
Composition and properties of the catalysts.

Catalyst	P, [a] wt.%	Pd, [a] wt.%	SSA, [b] m^2 g^{-1}	V_p, [b] cm^3 g^{-1}	CO, [c] μmol g^{-1}	D_{Pd}, [c] %	d_{Pd}, [c] nm
Pd/Al_2O_3	0.0	0.45	212	0.52	18.5	86	1.3
Pd/Al_2O_3-1P	0.9	0.46	183	0.46	15.1	70	1.6
Pd/Al_2O_3-2.5P	2.6	0.46	167	0.43	16.0	74	1.5
Pd/Al_2O_3-5P	5.4	0.47	132	0.36	16.4	74	1.5

[a] From ICP-OES analysis. [b] Specific surface area (SSA) determined from the N_2 adsorption isotherm using the BET method; the total pore volume (V_p) determined using the Gurvich method from the adsorption capacity at $p/p_0 = 0.95$. [c] Determined by pulse CO chemisorption method; Pd dispersion (D_{Pd}) was calculated assuming 1 to 2 CO to Pd adsorption stoichiometry [12]; the average Pd particle size (d_{Pd}) was calculated by Eq. (1).

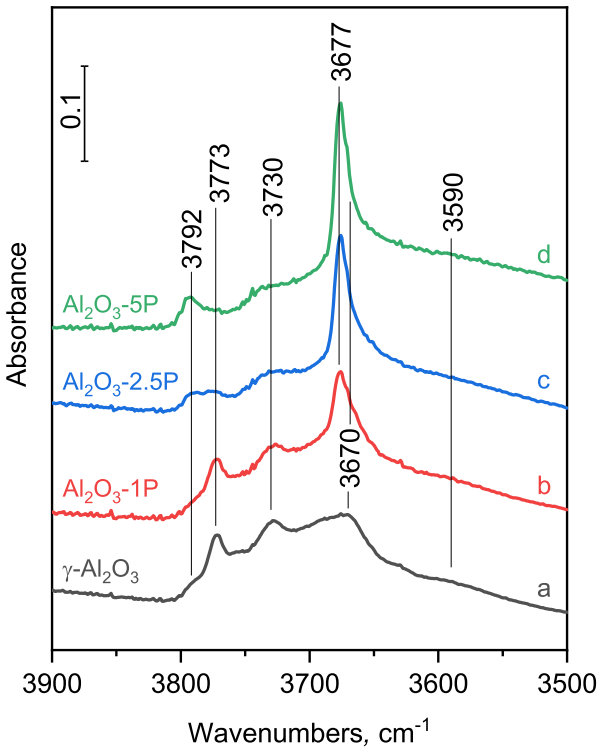

Fig. 2. FT-IR spectra of the ν_{OH} stretching region of (a) parent γ–Al_2O_3, and (b) Al_2O_3–1P, (c) Al_2O_3–2.5P, and (d) Al_2O_3 5P phosphatized alumina supports. The samples were pretreated in situ in the IR cell at 450 °C under high vacuum for 1 h.

very broad feature around 3590 cm^{-1} can be attributed to triply bridging OH species or OH groups in hydrogen bonding interactions [15–17].

The intensity drop of the OH bands (Fig. 2, b-d) clearly indicates OH consumption in a reaction with phosphoric acid. The reaction has been described as sort of surface acid-base neutralization reaction resulting in the formation of surface phosphate species and water [19–21]. The formation of phosphate species is clearly indicated by the appearance of the band at 3677 cm^{-1}, assigned to the ν_{OH} vibration of P–OH species (Fig. 2, b-d) and a strong $\nu_{P=O}$ vibrational band of the phosphate groups in the range of 1150–1250 cm^{-1} frequency (not shown). Interestingly, the characteristic ν_{OH} band of the terminal OH groups on tetrahedral aluminum ions at 3792 cm^{-1} gained in intensity as the concentration of the surface phosphate species increased (Fig. 2, a-d), suggesting that a surface reaction between phosphoric acid and alumina surface is not a simple acid-base neutralization reaction.

3.2.2. Surface basicity

The surface basicity of the phosphate-free and phosphatized γ–Al_2O_3 supports was characterized by the carbonate-like surface species obtained from CO_2 adsorption. The IR spectrum of these species was recorded and the spectral features were assigned on the basis of the available literature [17,21,22] (Fig. 3). The CO_2 uptake of the supports resulted mainly in the formation of two types of bicarbonate species as indicated by the appearance of the asymmetric $\nu_{O-C=O}$ vibrations at 1645 cm^{-1} for both B1 and B2 type bicarbonate species and the symmetric vibrations at 1454 cm^{-1} of the B1 and 1482 cm^{-1} of the B2 type bicarbonate species (Fig. 3A). The corresponding ν_{OH} bands of the bicarbonate species appear as positive bands at 3610 (B2 type) and 3595 cm^{-1} (B1 type, as a shoulder) in the range of the O–H vibration frequencies (Fig. 3B). The most intense negative ν_{OH} bands at 3773 and around 3700 cm^{-1} (Fig. 3B) suggest that mainly those OH groups were involved in the formation of bicarbonates, which have a coordinately unsaturated tetrahedral or octahedral aluminum atom in their neighborhood. Note that the involvement of these hydroxyl groups in the CO_2 adsorption could be just due to their location near to Lewis acid sites [16]. The lack of negative band at 3677 cm^{-1}, where the ν_{OH} band of the phosphorus–bound hydroxyls appears, implies that the P–OH groups do not participate in bicarbonate formation (Fig. 3B). In harmony with the conclusion of other authors [21,23], this result permitted for us to conclude that phosphatization does not generate basic centers for CO_2 uptake, i.e., the P–OH group is stronger acid than the CO_2.

The CO_2 uptake on the supports results also in the formation of bidentate chelating carbonate that gives weak IR band at 1670 cm^{-1} (shoulder) and monodentate carbonate bands at 1542 and 1404 cm^{-1} (shoulders) frequencies (Fig. 3A) [17,22]. Formation of these carbonate species probably takes place with the involvement of coordinately unsaturated aluminum cation and oxide anion pairs, which oxide ions are Lewis base sites on the alumina surface [16,17,21]. It is important to note that the strength of the characteristic absorption bands of the carbonate species is inversely proportional to the phosphate loading (Fig. 3A, a-d). These results suggest that formation of phosphate species is accompanied not only by consumption of basic surface OH groups, but also by elimination of Lewis base sites.

The concentration and distribution of basic sites on the parent and phosphatized γ–Al_2O_3 supports were determined by CO_2-TPD measurements. The TPD curves in Fig. 4 indicate the presence of at least three overlapping component bands. According to Wang et al. [22], a peak appearing around 80 °C is due to the decomposition of bicarbonate species formed on weak basic sites, whereas the component peaks observed around 160 and 250 °C can be attributed to decomposition of chelating bidentate carbonate species formed on medium strength basic sites and monodentate carbonate species formed on strong basic sites, respectively. These assignements are clearly supported by the observed thermal stability of different carbonate species (Fig. S2). An additional high temperature peak, attributed to bridging bidentate carbonate species formed on strong basic sites, may also appear at around 325 °C temperature. Therefore, the CO_2-TPD curves shown in Fig. 4 were resolved by peak fitting using four component peaks. The peak fitting process resulted essentially in three major component peaks with a maximum around 85, 135, and 220 °C, representing weak, medium strength and strong basic sites (the fourth component peak had a negligible intensity on each sample, therefore it was ignored). The total amount of different basic sites and their distribution was calculated from the area under the corresponding curves using the result of a previous calibration measurement (Table S1). The concentrations of the weak-to-moderate strength basic sites and the strong basic sites are listed in Table 2. Results show that introduction of phosphate groups significantly decreased the concentration of all types of basic centers on the surface of the alumina support, which dropped by more than 90 % for the support, having the highest phosphorous content.

3.2.3. Surface acidity

Adsorption of Py on the Lewis acid sites of alumina results in the formation of coordinately bonded Py giving absorption bands in the range of 1630–1590 (8a band) and 1460–1430 cm^{-1} (19b band) [16,17,25]. The pair of bands observed at 1623 and 1456 cm^{-1} in Fig. 5a can be assigned to Py adsorbed on tricoordinated Al^{3+} cations (tetrahedral Al cations with coordinative unsaturation), which represent the strongest acid Lewis sites of alumina. The second pair of bands at 1615 and 1451 cm^{-1} can be also attributed to Py adsorbed on Al ions with coordinative unsaturation, which are most probably in octahedral coordination

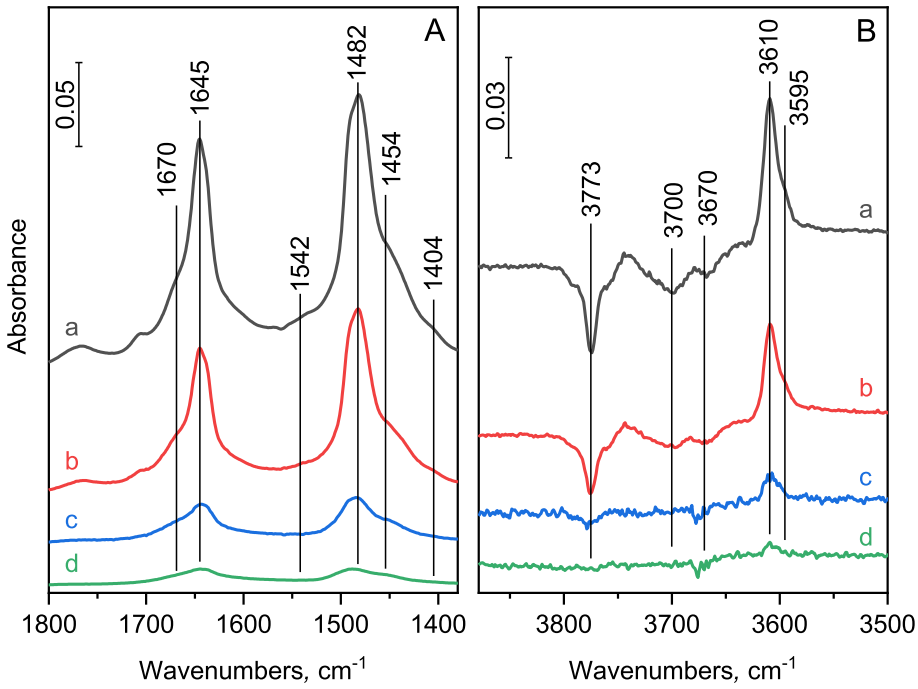

Fig. 3. FT-IR spectra of (A) surface species formed from CO_2 on the parent γ–Al_2O_3 (a) and on the Al_2O_3–1P (b), Al_2O_3–2.5P (c), and Al_2O_3–5P (d) phosphatized alumina supports and (B) the corresponding difference spectra in the range of the O–H stretching vibrations. Samples were pretreated in situ in the IR cell at 450 °C under high vacuum for 1 h then were contacted with 15 mbar of CO_2 at room temperature for 30 min. Spectra were taken after 30 min evacuation at room temperature.

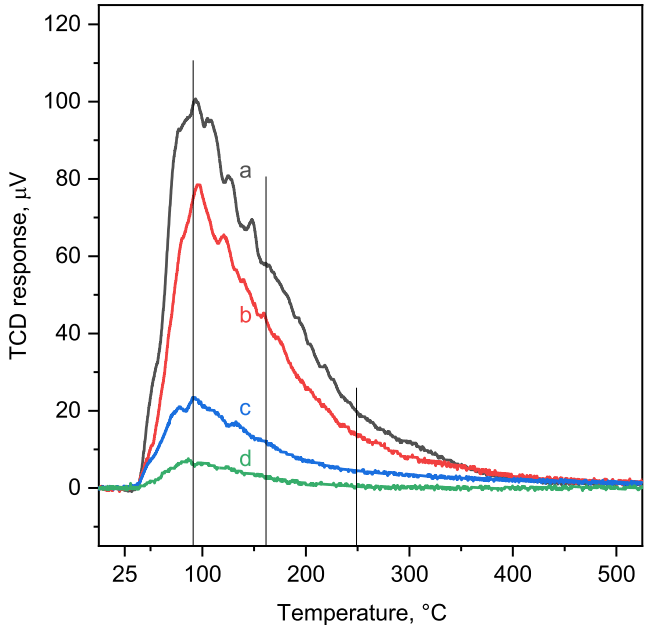

Fig. 4. CO_2-TDP curves measured for (a) parent γ–Al_2O_3, and (b) Al_2O_3–1P, (c) Al_2O_3–2.5P, and (d) Al_2O_3–5P phosphatized alumina supports. Prior to the CO_2-TPD run the sample was activated in O_2 stream at 550 °C. Adsorption was carried out at room temperature at 133 mbar CO_2 pressure. The TPD run was performed in He flow at a heating rate of 10 °C min^{-1} up to 700 °C.

[16,17,25] and represent weaker acid Lewis sites than those of the coordinately unsaturated tetrahedral aluminum cations.

The spectra of adsorbed CO_2 support above identification of Py sorption sites. Bands at 2360 and 2345 cm^{-1}, which belong to the so called Σ_u^+ mode of linearly coordinated (end-on adsorbed) CO_2 [17,21,26], were found to develop in the presence of CO_2 gas in the IR cell (Fig. S3). These bands are most probably bands of CO_2, bound to strong and weak, coordinately unsaturated Lewis acid Al centers in tetrahedral and octahedral coordination, respectively.

The intensity of Py bands is lower for the supports having higher phosphate concentration (Fig. 5, a-d), suggesting that formation of surface phosphate affected the concentration of both types of Lewis acid sites.

The bands of linearly adsorbed CO_2 are also weaker for the phosphatized supports, indicating that surface phosphate eliminates Lewis acid sites of alumina (Fig. S3, a-d).

Evacuation at 400 °C resulted in the total desorption of Py from the weaker Lewis acid sites (see the intensity drop of the bands at 1615 and 1451 cm^{-1}), whereas the strongest Lewis acid sites still withheld Py (see the bands at 1623 and 1456 cm^{-1}) (Fig. 5, dashed lines). Assuming that the total number of Lewis sites and the number of strong Lewis sites are proportional to the band intensities observed after evacuation at 100 °C and 400 °C, respectively, the corresponding concentrations of Lewis acid sites were determined by using the extinction coefficient given in ref. [24]. The concentrations of the weak-to-moderate strength Lewis acid sites and the strong Lewis acid sites are listed in Table 2.

3.2.4. ^{31}P MAS NMR and ^{1}H-^{27}Al CP/MAS NMR results

The type of surface phosphate species was detected by ^{31}P MAS NMR. The spectrum of the Al_2O_3–1P sample, having the lowest P content, shows peaks at −10 and −22 ppm (Fig. 6A, b), which peaks can be assigned to phosphorous in monomeric and polymeric phosphate species, respectively [22,23,27,28]. At higher phosphorous contents, both peaks were stronger, while the peak of the polymeric species gained even more intensity (Fig. 6A, b-d). In line with expectations [23], the higher surface phosphate concentration favors the formation of polymeric species via condensation of P–OH groups.

The changing local environment of aluminum atoms on the surface of alumina upon phosphate modification was characterized by ^{1}H and ^{27}Al CP/MAS NMR (Fig. 6B). The ^{1}H spectra reflect the local environment of those Al atoms which are near to protons at the

Table 2
Basicity and acidity of the catalyst supports.

Support	Basic sites,[a] μmol g^{-1}		Lewis acid sites,[b] μmol g^{-1}	
	Weak-to-medium	Strong	Weak-to-medium	Strong
γ-Al_2O_3	90.8	34.7	16.1	4.47
Al_2O_3-1P	66.0	26.3	16.7	4.37
Al_2O_3-2.5P	22.8	8.2	14.9	2.35
Al_2O_3-5P	5.8	1.3	12.9	1.90

[a] Determined from the CO_2-TPD measurements. Weak and medium strong basic sites were determined from the component peaks at 85 and 135 °C, whereas that of strong basic sites from the component peak at 220 °C. [b] Calculated from the Py adsorption examined by FT-IR spectroscopy. Concentration of Lewis acid sites was calculated from the integrated absorbance of the 1450 cm^{-1} Py band after degassing the wafer at 100 °C (weak and medium strength Lewis acid sites) and 400 °C (strong acid Lewis sites), respectively. For the calculation, the integrated molar extinction coefficient of 2.22 cm μmol^{-1} was used [24].

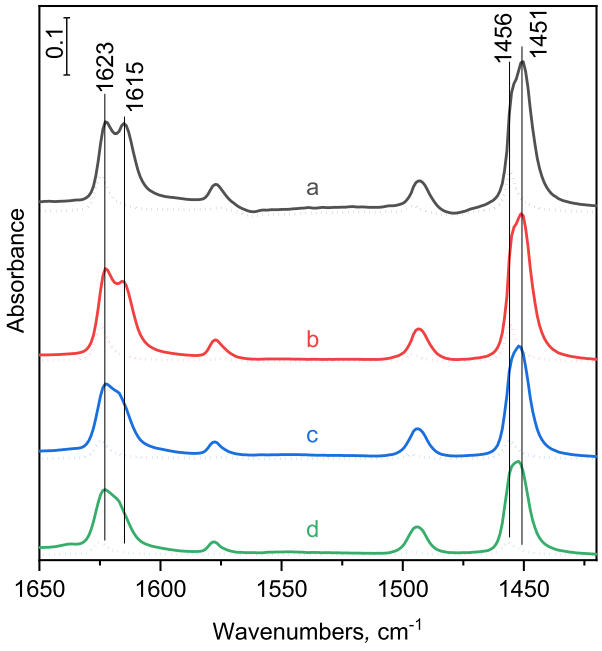

Fig. 5. FT-IR spectra of surface species formed from adsorption of Py on (a) parent γ–Al_2O_3, and (b) Al_2O_3–1P, (c) Al_2O_3–2.5P, and (d) Al_2O_3–5P phosphatized alumina supports. Samples were pretreated in situ in the IR cell at 450 °C under high vacuum for 1 h then were contacted with 5 mbar of Py vapor at 200 °C for 30 min. Spectra were taken after evacuation at 100 °C for 30 min (thick solid lines) and then after evacuation at 400 °C for 30 min (thin dotted lines).

surface or near to surface-attached OH groups [23,29]. On the parent alumina support ^{27}Al resonance peaks can be observed at 14, 38, and 75 ppm (Fig. 6B, a), which can be attributed to octahedral (Al^{VI}), pentagonal (Al^{V}), and tetrahedral (Al^{IV}) surface aluminum atoms [27–30]. Note that pentagonal aluminum atoms (Al^{V}) are often observed in high surface area transition aluminas in minor concentrations and their presence is associated with oxygen defects adjacent to aluminum nucleus or substitution of lattice oxygen in octahedral symmetry by hydroxyl groups [30,31]. When the alumina surface was modified with increasing amount of phosphate, it was clearly visible that relatively broad component peaks developed at lower chemical shifts near to these peaks at about 54, 26, and 5 ppm (Fig. 6B, b-d) indicating the changes in the local environment of the corresponding surface Al atoms due to the formation of Al-O-P bonds [27,32]. Results show that all types of surface Al atoms were involved in the formation of Al-O-P bonds, suggesting the non-selective binding of the phosphate to the alumina surface. This observation is in line with the spectral changes found in the ν_{OH} region (Fig. 2) indicating the consumption of all the different types of OH groups upon phosphating the alumina surface.

3.2.5. Characterization of the Pd surface by CO chemisorption

It is generally accepted that the carbonyl bands of CO adsorbed on highly dispersed Pd catalysts appear in the spectral range below and above about 2000 cm^{-1}, attributed to bridging and linearly-bound CO, respectively [12,33,34]. The FTIR spectrum of the species formed from CO adsorption on alumina-supported Pd catalysts are shown in Fig. 7. Carbonyl bands are clearly discernible at about 1860, 1945, 2050, and 2085 cm^{-1}. Following the band assignments of Lear et al. [34,35], the broad band at about 1860 cm^{-1} can be assigned to μ_3 hollow-bonded CO on Pd [111] planes or μ_2 bridge-bonded CO on Pd [100] planes, whereas the band near to 1945 cm^{-1} can be attributed to the μ_2 bridge-bonded CO on Pd [100] facets and CO, bridge bonded to particle edges. The linear CO peaks at around 2050 and 2085 cm^{-1} can be ascribed to CO bound to Pd [111]/[111] and Pd [111]/[100] particle edges, and CO bound to particle corners, respectively [34,35]. These bands are all present both on the non-phosphatized and phosphatized-alumina-supported Pd catalysts, although some deviation from the published relative intensities, are apparent (Fig. 7). In particular, the linear features relative to the bridge-bonded features became more pronounced at increasing phosphorous content of the support, which suggest somewhat greater contribution of the Pd particle edges and corners to the adsorption. Note that phosphating the alumina support hardly affected the metal dispersion and the Pd particle size in the catalysts (Table 1).

3.3. Catalytic activity

Results of catalytic hydroconversion of tricaprylin (TC) are shown in Fig. 8. The organic liquid product contained the unreacted TC (if any) and caprylic acid, propyl caprylate, 1-octanol, octyl caprylate, heptane, octane, and some other minor products, mainly octanal, 8-pentadecanon, 9-nonanone, and dicaprylates formed by the hydrogenolysis of only one ester bond of TC. Caprylic acid and propyl caprylate is formed by the hydrogenolysis (HYS) reaction of three or two ester bonds, respectively, whereas octyl caprylate could have been formed by esterification of caprylic acid by octanol. Heptane and octane were produced via deoxygenation of caprylic acid. Octanol is a possible intermediate of paraffin formation [11]. The effluent gas contained mainly propane (from HYS reaction) and CO. Minor amounts of CO_2, ethane, and methane could be also detected. The dominance of heptane over octane and CO over CO_2 in the liquid and gas phase product mixture, respectively, suggests that hydrodecarbonylation (HDCO) is the main deoxygenation route, whereas hydrodecarboxylation (HDCO2) and oxygen hydrogenation (HDH2O) represent minor reaction routes [6,7].

At the reaction temperature of 300 °C the conversion of TC was low (18.5 %) on the Pd/Al_2O_3 catalyst, but reached virtually 100 % on the Pd/Al_2O_3–2.5P and Pd/Al_2O_3–5P catalysts (Fig. 8, left side). When the reaction temperature was raised to 350 °C, all the

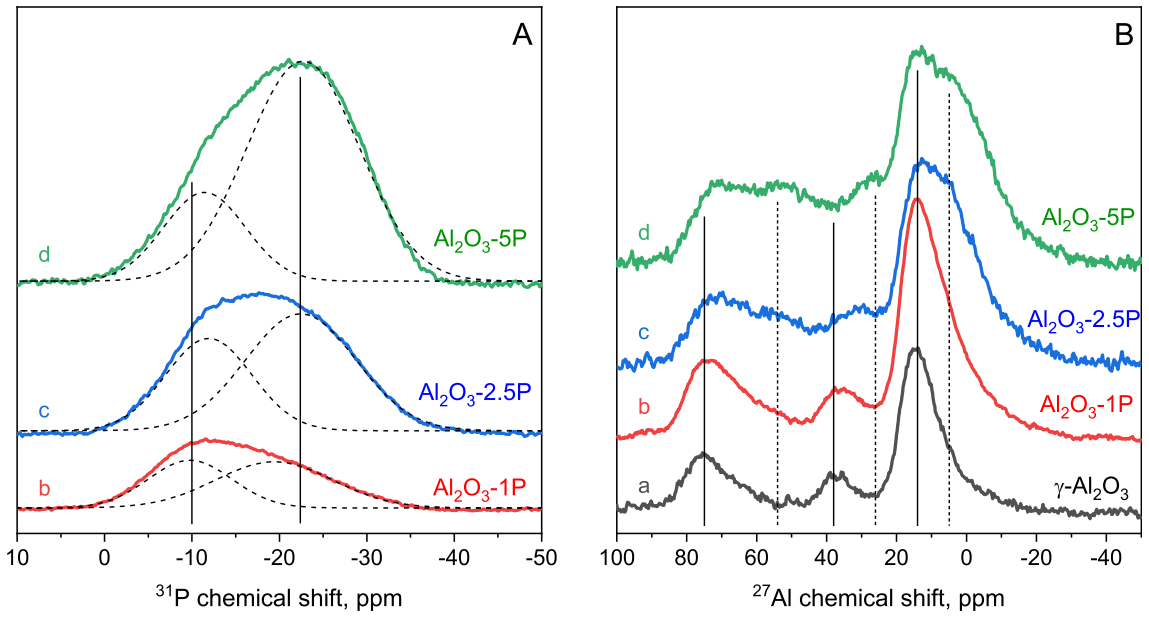

Fig. 6. ^{31}P MAS NMR (A) and ^{1}H-^{27}Al CP/MAS NMR (B) spectra of (a) parent γ–Al_2O_3, and (b) Al_2O_3–1P, (c) Al_2O_3–2.5P, and (d) Al_2O_3–5P phosphatized alumina supports.

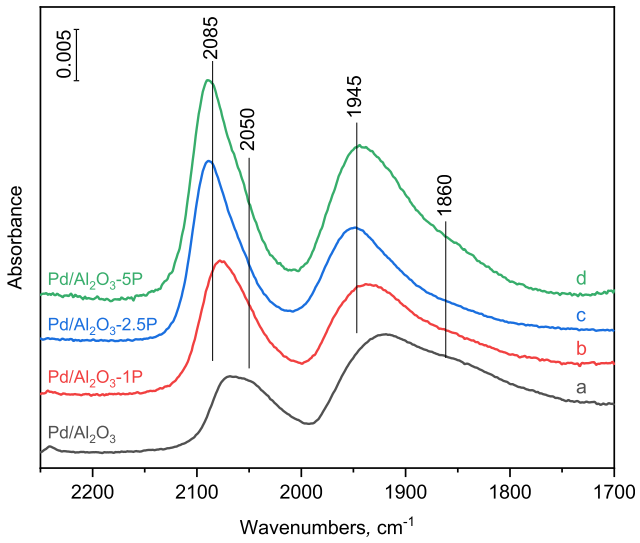

Fig. 7. FT-IR spectra of adsorbed species formed from carbon monoxide on (a) Pd/Al_2O_3, (b) Pd/Al_2O_3–1P, (c) Pd/Al_2O_3–2.5P, and (d) Pd/Al_2O_3–5P catalyst samples. Samples were pretreated in situ in the IR cell at 450 °C in H_2-flow for 1 h then contacted with 5 mbar of CO at room temperature for 30 min. Spectra were taken after removing gas phase CO from the cell by evacuation at room temperature.

phosphatized-alumina-supported Pd catalysts showed high activity in the HYS reaction resulting in 100 % TC conversion (Fig. 8, right side). In line with earlier findings [11], these results suggest that caprylic acid intermediate was formed by facile HYS reaction from TC, which was followed by consecutive, rate-limiting deoxygenation (mainly HDCO) reaction of the intermediate. Interestingly, the yield of the paraffin products (heptane and octane) dramatically increases with the phosphorous content of the alumina support reaching nearly 100 % on the Pd/Al_2O_3–5P catalysts (Fig. 8, right side). These results clearly suggest that phosphatization of alumina surface resulted in the change of catalyst structure so that the rate of the hydrodeoxygenation (mainly HDCO) reaction was significantly enhanced.

3.4. In situ DRIFT spectroscopic investigation

The carboxylate species formed from adsorption of valeric acid, and their reactivity was investigated under catalytic conditions by quasi-operando DRIFT spectroscopy. The results obtained for the Pd/Al_2O_3 and Pd/Al_2O_3–5P catalysts are presented in Figs. 9 and 10, respectively.

Molecularly adsorbed carboxylic acid could not be observed under the conditions of experiments, i.e., the characteristic $\nu_{C=O}$ band of valeric acid expected to appear at ~ 1780 cm^{-1} could not be detected. The negative bands in the ν_{OH} region (Figs. 9-10, Section A) and positive bands in the ν_{O-C-O} region (Figs. 9-10, Section B) clearly suggest that the adsorption of the carboxylic acid resulted in the consumption of surface OH groups and in the simultaneous formation of surface carboxylate species [36,37]. This surface reaction (dissociative adsorption) is described as the deprotonation of the carboxylic acid by the combination of acid hydrogen with a surface hydroxyl group to produce surface carboxylate species and H_2O [36–38]. Results shown in Fig. 9A and 10A indicate that practically all types of OH groups on the support can be involved in the formation of carboxylate species, including the P–OH groups of the phosphatized support (Fig. 2). Note that phosphatization resulted in consumption of surface Al–OH groups and formation of new P–OH groups (Fig. 2). Both the remaining Al–OH and the new P–OH groups are available for the adsorption of carboxylic acid and their total number determines the surface concentration of the carboxylate groups.

The position of the asymmetric and symmetric ν_{O-C-O} stretching bands appearing over and below about 1500 cm^{-1}, respectively, in addition to the difference between their peak positions ($\Delta\nu = \nu_{as}$-ν_s) are indicative of the bonding structure of carboxylate species [36,37,39,40]. The frequency of the ν_{as} vibration and the corresponding $\Delta\nu$ value were shown to increase in the following order: chelating bidentate < bridging bidentate (≈ free ionic) < monodentate carboxyl species. The intense pair of bands observed at 1575 and 1470 cm^{-1} ($\Delta\nu$ = 105 cm^{-1}) for the Pd/Al_2O_3 sample (Fig. 9B) and a similar pair of bands at 1585 and 1470 cm^{-1} ($\Delta\nu$ = 115 cm^{-1}) for the Pd/Al_2O_3–5P sample (Fig. 10B) can be assigned to the asymmetric and symmetric vibrations of chelating bidentate carboxylate species [36,37,39,40]. A

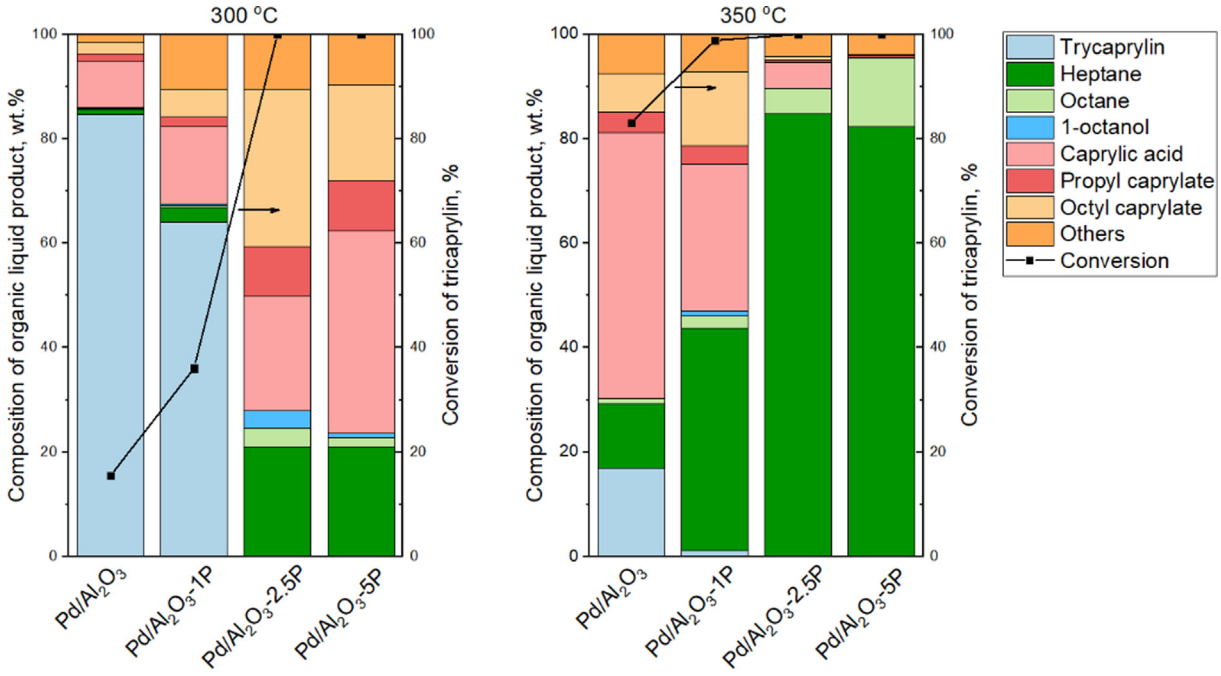

Fig. 8. Catalytic hydroconversion of tricaprylin over Pd catalysts supported on parent γ–Al_2O_3, and on the Al_2O_3–1P, Al_2O_3–2.5P, and Al_2O_3–5P phosphatized alumina supports. Catalysts were pretreated in situ in H_2-flow at 450 °C at atmospheric pressure. Catalytic tests were carried out at 300 °C (left) or 350 °C (right) at a total pressure of 21 bars and at a WHSV of $4 g_{tricaprylin} g^{-1}_{catalyst} h^{-1}$, whereas the H_2/tricaprylin molar ratio was 20.

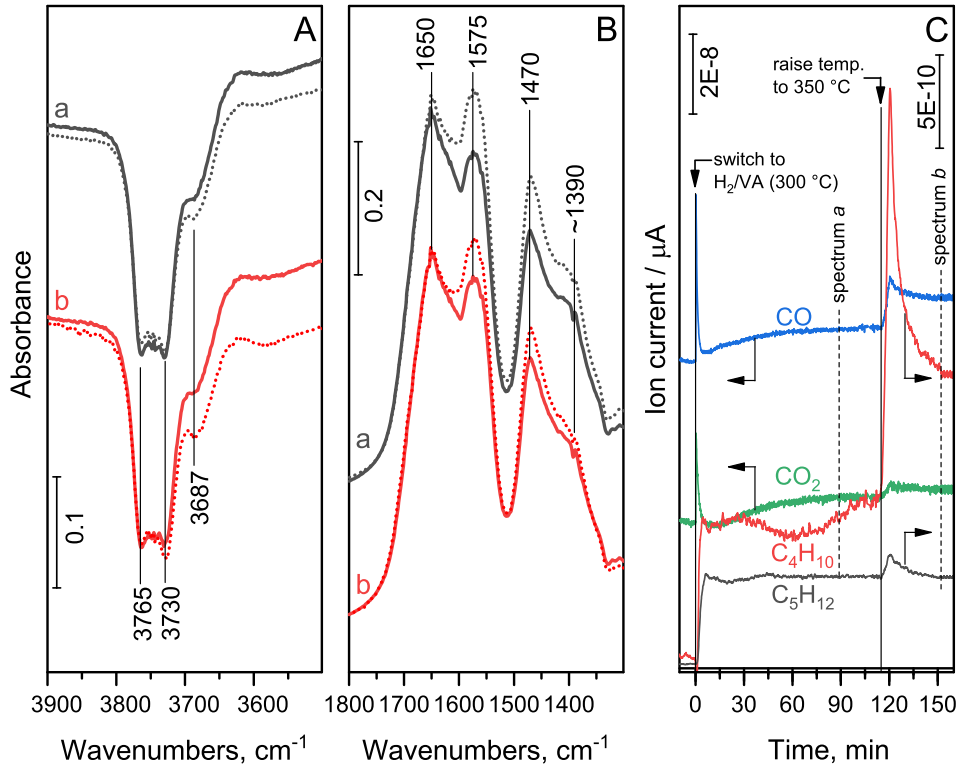

Fig. 9. Difference DRIFT spectra in the range of the (A) O–H stretching and (B) C = O stretching and C–H deformation vibrations on the Pd/Al_2O_3 catalyst in contact with (a) He/valeric acid mixture (dotted lines) or H_2/valeric acid mixture (solid lines) at 300 °C or (b) at 350 °C. Part (C) shows the MS signals characteristic of CO, CO_2, butane, and pentane as HDO products in the effluent gas from the DRIFT reactor cell during the operando DRIFTS experiment with H_2/valeric acid mixture. Dashed lines indicate the point where spectra were collected after reaching the steady state at the given reaction temperature.

second type of carboxylate species gives an intense asymmetric ν_{O-C-O} stretching band at 1650 cm^{-1} (Fig. 9B). The identification of its symmetric pair is, however, difficult due to the appearance of overlapping C–H deformation vibrations in the frequency range below 1500 cm^{-1}, most probably due to the appearance of the $\delta_{as}(CH_3)$, $\beta_s(CH_2)$, and $\delta_s(CH_3)$ vibrations of the $-CH_3$ and $-CH_2-$ groups of

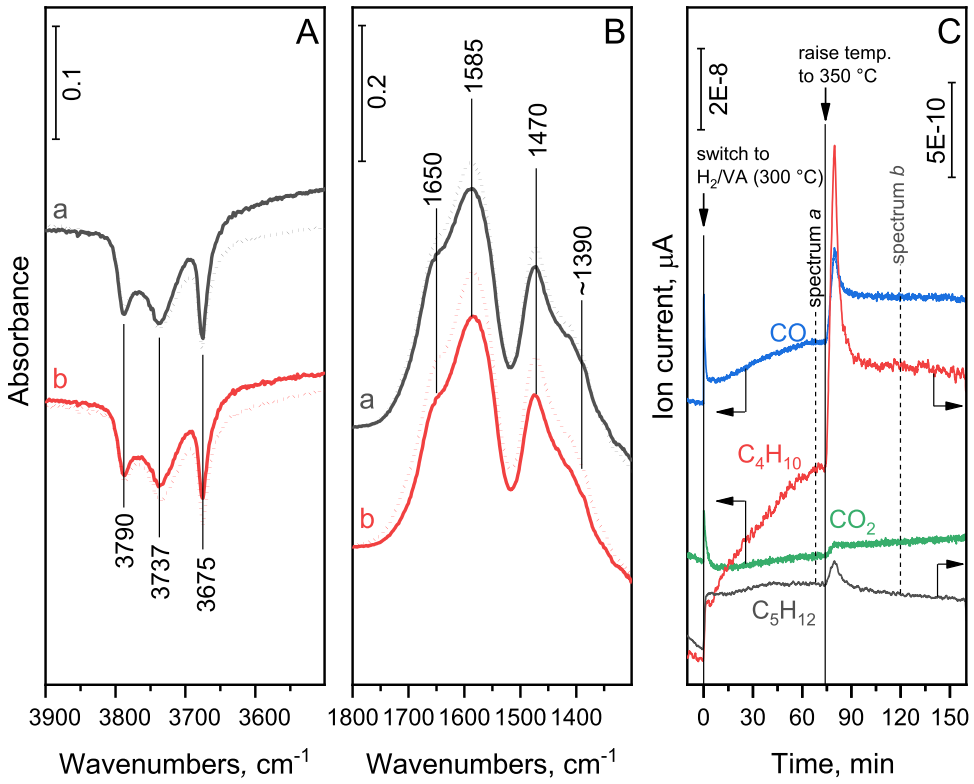

Fig. 10. Difference DRIFT spectra in the range of (A) O-H stretching and (B) C = O stretching and C–H deformation vibrations on Pd/Al_2O_3–5P catalyst in contact with He/valeric acid mixture (dotted lines) or H_2/valeric acid mixture (solid lines) at (a) 300 °C and (b) 350 °C. Part (C) shows the MS signals characteristic of CO, CO_2, butane, and pentane as HDO products in the effluent gas from the DRIFT reactor cell during the operando experiment with H_2/valeric acid mixture. Dashed lines indicate the point where spectra were collected after reaching the steady state at the given reaction temperature.

the hydrocarbon chain (the $\delta_s(CH_3)$ vibration is clearly discernible at around 1350 cm^{-1}) [36,40,41]. However, we found a band at about 1390 cm^{-1} that showed parallel of intensity with that of the 1650 cm^{-1} band, if reaction conditions were varied. It was substantiated that a band at about 1390 cm^{-1} is the pair of the 1650 cm^{-1} band, stemming from symmetric $\nu_{O\text{-}C\text{-}O}$ stretching vibration (Fig. 9B, 10B, and S4, S5). The relatively high frequency of the asymmetric $\nu_{O\text{-}C\text{-}O}$ vibration band (1650 cm^{-1}) and the large frequency separation from the corresponding symmetric vibration band ($\Delta\nu$ = 1650 – 1390 = 260 cm^{-1}) clearly suggest that this second type of carboxylate group can be identified as monodentate carboxylate species bonding to surface aluminum atom [39,40]. Note that the concentration of the monodentate carboxylate species is much lower over the Pd/Al_2O_3–5P sample than over the Pd/Al_2O_3 sample (Fig. S4, Sections C and D). Phosphatization of γ–alumina surface eliminated mainly those sites, where monodentate carboxylate species could have been formed.

Upon contacting the catalysts with He/VA mixture at 300 °C gradually carboxylate bands developed (Fig. S4) until their surface concentration reached steady state (Fig. 9B and 10B, spectra *a*). Virtually the same steady state concentrations were reached at 350 °C (Fig. 9B and 10B, spectra *b*). As expected, no reaction products were formed in the absence of H_2.

When the reactant flow was changed to H_2/VA, the intensity of the bands at 1575–1585 cm^{-1} and 1470 cm^{-1} decreased, suggesting that mainly the concentration of the corresponding bidentate carboxylate species decreased, whereas the surface concentration of the monodentate carboxylate species (bands at 1650 and 1390 cm^{-1}) hardly changed. The consumption of the bidentate carboxyl species was accompanied by the appearance of the main deoxygenation reaction products, such as, butane, pentane, CO and CO_2. Higher reaction temperature resulted in a higher reaction rate and, therefore, in higher product concentrations in the effluent gas (Fig. 9C and 10C). The dominance of butane and CO in the product mixture suggests that the main route of VA deoxygenation is the HDCO reaction. The results suggest that the surface of the Pd/Al_2O_3 catalyst is covered by more reactive bidentate carboxylate species and less reactive monodentate carboxylate species. In contrast, the surface coverage of the Pd/Al_2O_3–5P catalyst by the more active carboxylate is substantially higher, and it is much lower by the less active species than the corresponding coverages of the Pd/Al_2O_3 catalyst.

Product formation was accompanied by recovery of surface OH groups as indicated by the intensity drop of some negative OH bands (Fig. 9A and 10A). Because the reaction of carboxylic acid and OH groups is accompanied by release of H_2O, the recovery of OH groups had to involve C–O bond hydrogenolysis. Mainly lower-frequency OH groups recovered, showing that the less basic OH groups were involved in the formation of reactive carboxylates [16,17].

4. Discussion

The effect of phosphatization on the alumina surface seems to be twofold: it consumes surface Al–OH groups (Fig. 2) and also reduces the concentration of Lewis acid sites (Table 2) and consequently the concentration of the Lewis acid ($Al^{\oplus}$) – Lewis base ($O^{\ominus}$) pair sites. Note that latter oxygen atoms can behave as Brønsted base (proton acceptor) or Lewis base (electron pair donor) sites depending on the nature of the adsorbate [42].

The reaction of phosphoric acid with surface OH groups is well documented [20,21]. It is considered to be an acid-base reaction, as shown in Scheme 1A. The reaction results in the formation of surface phosphate groups and water. Phosphate species formed on

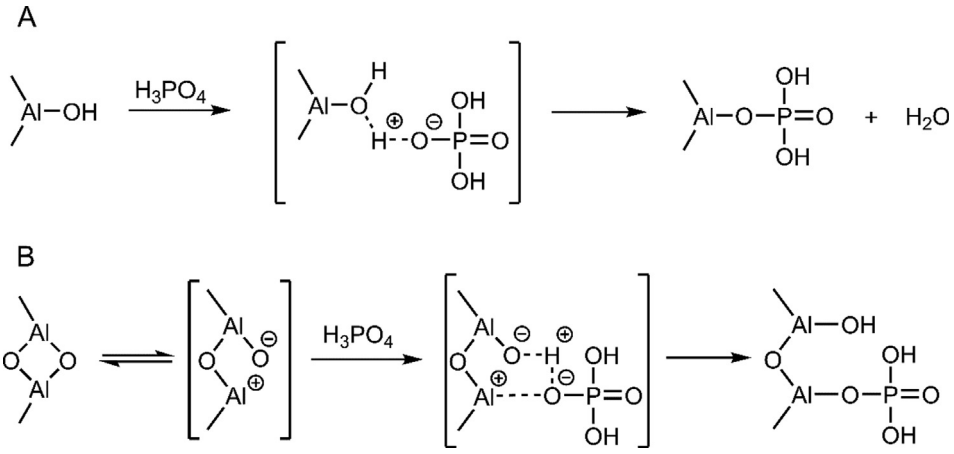

Scheme 1. Reaction of phosphoric acid with (A) surface OH groups, and (B) Lewis acid ($Al^{\oplus}$) – Lewis base ($O^{\ominus}$) pair sites.

adjacent OH groups can condensate via P–OH groups to form polymeric phosphate species [23], which appeared as dominating species at higher (≥2.5 wt%) phosphate loadings (Fig. 6A). It is important to note that phosphatization results not only in the appearance of P–OH groups but also in the formation of non-reactive terminal Al^{IV}-OH groups (Fig. 2). A similar phenomenon was observed in a former study and was related to the reaction between a bridging OH group (Al–O(H)–Al) and phosphoric acid giving a terminal OH group and a $[H_2PO_4]^-$ ligand attached to a surface Al atom [20]; however, it was not clarified how the charge neutrality was preserved in this process.

The present study evidenced that formation of new terminal Al^{IV}–OH groups was accompanied by the elimination of strong acid Lewis sites (i.e., coordinately unsaturated tetrahedral Al sites) and their charge balancing Lewis base (oxide ion) pair sites. We rationalize these observations by the reaction shown in Scheme 1B. The strong Lewis acid sites were suggested to become reversibly reconstructed by establishing a weak bond with a nearby oxide ion and thus they could appear more as a distorted tetrahedral ion than as a tri-coordinated one (see left side of Scheme 1B) [16]. However, the very weak coordination bond in the strained species can be easily broken in the presence of a base or an acid [16,43]. Our results substantiate that phosphoric acid reacts with these Lewis acid ($Al^{\oplus}$) – Lewis base ($O^{\ominus}$) pair sites resulting in the formation of terminal Al^{IV}-OH species and $[H_2PO_4]^-$ groups completing the coordination sphere of coordinately unsaturated tetrahedral Al sites (right side of Scheme 1B). Note that latter oxide ions behave as proton acceptor Brønsted base sites in the process, whereas the $[H_2PO_4]^-$ groups cannot be distinguished from those formed with the involvement of surface OH groups (vide supra). The process proposed here clearly indicates how the charge neutrality can be maintained during the formation of the terminal OH groups, and also accounts for the elimination of Lewis acid ($Al^{\oplus}$) – Lewis base ($O^{\ominus}$) pair sites (Scheme 1B). This is in line with the suggestion of DeCanio et al. [43] for the bonding of fluoride ions to strong Lewis acid sites upon HF treatment of alumina support.

The quasi-operando DRIFTS investigation revealed the formation of two types of surface carboxylate species under catalytic conditions (Figs. 9-10). Bidentate carboxylate species were formed via acid-base reaction between fatty acid and a surface hydroxyl groups to produce stable surface carboxylate and H_2O as shown in Scheme 2A [36–38]. It is most likely that the generated water desorbs from the surface at the reaction temperatures (300 and 350 °C) applied here during the DRIFTS investigations [37]. This process shows close resemblance to that observed for the surface

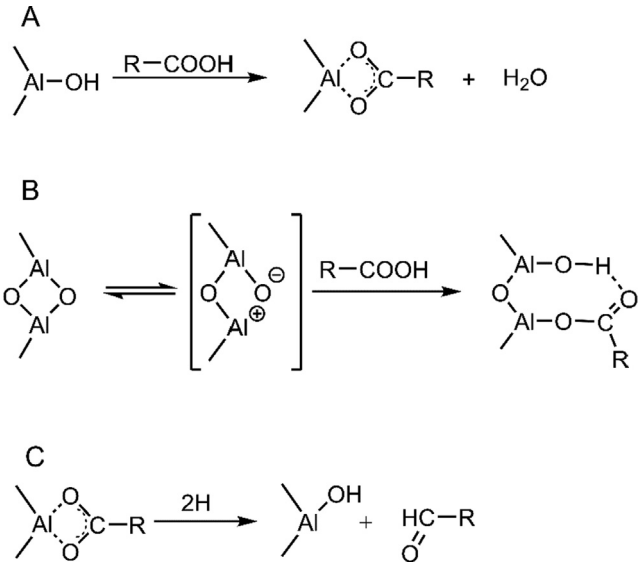

Scheme 2. Formation of carboxylate species via the reaction of carboxylic acid with (A) surface OH groups, (B) Lewis acid ($Al^{\oplus}$) – Lewis base ($O^{\ominus}$) pair sites, and (C) possible formation of aldehyde intermediate from bidentate carboxylate species.

reaction with phosphoric acid (see above and in Scheme 1A). The second type of carboxylate could be identified as monodentate carboxylate group [39,40]. It is rational to think that these latter species were formed in a similar process over Lewis acid ($Al^{\oplus}$) – Lewis base ($O^{\ominus}$) pair sites than that we proposed for the surface reaction with phosphoric acid (cf. Scheme 1B and 2B). The result is a monodentate carboxylate group, in which one of the oxygen forms an ester-like bond with a surface aluminum atom, while the other oxygen forms an H-bond with the neighboring OH group (right side of Scheme 2B) [39,44]. The reactive adsorption of carboxylic acid on strong Lewis acid ($Al^{\oplus}$) – Lewis base ($O^{\ominus}$) pair sites is clearly supported by the good correlation between the concentration of strong Lewis acid sites (determined by Py adsorption) and the integrated absorbance values of the asymmetric $\nu_{O\text{-}C\text{-}O}$ band at 1650 cm^{-1}, assigned to monodentate carboxylate species (Table S2).

In relation to the catalytic properties, the most important consequence of phosphatization is that it reduces the concentration of $Al^{\oplus}$– $O^{\ominus}$ pair sites, where the less reactive monodentate carboxylate species are formed. The DRIFTS investigations showed that both types of carboxylates are strongly-bound surface intermedi-

ates, but the bidentate carboxylate species are more susceptible to deoxygenation reaction leading to paraffin product than the monodentate carboxylate intermediate (Figs. 9 to 10). The dominance of the bidentate carboxyl species on the phosphatized alumina support explains the substantially higher deoxygenation (mainly HDCO) activity of the phosphate catalyst as compared to the Pd/Al_2O_3 catalyst (Fig. 8). Note that phosphatization did not affect noticeably either the particle size, or the morphology of the Pd particles, therefore the enhanced deoxygenation activity and paraffin selectivity can be attributed to changes in the surface properties of the alumina support. Nevertheless, the reaction between the active surface intermediate and hydrogen most probably should take place at the metal/support interface where activated hydrogen is available for the reaction.

We found that preferentially weak base OH groups were recovered during the HDO reaction (Fig. 9A and 10A). The recovery of surface OH groups must involve the scission of a carboxylate C–O bond. The most likely product is aldehyde (Scheme 2C), which is considered as an important intermediate of the HDO reaction of carboxylic acids [2,5,8]. Note that the process depicted in Scheme 2C is the reverse process than that observed for surface carboxyl formation from aldehyde on metal oxides [36]. Our results suggest that the bidentate carboxylate species, formed in reaction with weak base hydroxyls, are more ready to react with hydrogen than the carboxylates formed in reaction with strong base surface sites. In this context, replacement of OH groups by P–OH groups favorably affects the HDO activity.

Paraffin formation proceeds mainly via hydrodecarbonylation (HDCO) of the aldehyde intermediate, whereas oxygen reduction reaction (HDH2O) of aldehyde represents a minor reaction route. The paraffin chain of fatty acids is shortened in HDCO but it is preserved in HDH2O reaction [2,5,7]. This latter reaction was suggested to proceed via primary alcohol intermediate and requires hydrogenation, dehydration, and/or hydrogenolysis steps [2,8]. One can speculate that latter reaction goes on a less complex reaction pathway in which the cleavage of both C–O bonds in the surface carboxylate species occurs, however, the justification of such reaction route still requires further investigation.

5. Conclusions

This study provides insights into the structure – activity relationships, determining the triglyceride HDO activity of alumina-supported Pd catalysts. The Pd/γ-A_2O_3 catalyst showed relatively good activity in the ester bond hydrogenolysis of triglyceride, but poor activity in the consecutive deoxygenation of the obtained carboxylic acid intermediate to paraffin product.

Surface modification of the γ-alumina support with phosphate resulted in surprisingly high activity enhancement of the catalyst in the later rate-determining step of paraffin formation. The phosphatization of the alumina surface resulted in (i) partial elimination of basic Al–OH groups and the concomitant formation of weak acid P–OH groups on the alumina surface, (ii) a decrease in the number of Lewis acid ($Al^{\oplus}$) – Lewis base ($O^{\ominus}$) pair sites, whereas (iii) it did not affect noticeably either the particle size, or the morphology of the Pd particles on the support.

Quasi-operando DRIFTS investigation under catalytic conditions revealed that both surface Al–OH and P–OH groups serve as sites for fatty acids to form bidentate carboxylate groups, which can further react with hydrogen to form paraffin products. If the OH groups, involved in the carboxylate formation are less basic, the formed carboxylate groups are more ready to react with hydrogen.

Carboxylic acids can also react with strong Lewis acid ($Al^{\oplus}$) – Lewis base ($O^{\ominus}$) pair sites giving monodentate carboxylate species, having low reactivity. Since phosphatization significantly reduced the number of these pair sites, the concentration of the less reactive monodentate carboxylate groups decreased substantially. The dominance of reactive bidentate carboxylate groups on the phosphatized alumina surface explains the substantially higher HDO, mainly hydrodecarbonylation (HDCO) activity of the phosphatized-alumina-supported Pd catalyst than the HDO activity of the Pd/γ–Al_2O_3 catalyst.

The product formation from the bidentate carboxylate surface intermediate is accompanied by OH group recovery, suggesting that the deoxygenation reaction must start with the hydrogenolysis of a carboxylate C–O bond. This reaction leads to the formation of aldehyde that must be the intermediate of deoxygenation to paraffin.

Declaration of Competing Interest

The authors declare that they have no known competing financial interests or personal relationships that could have appeared to influence the work reported in this paper.

Acknowledgements

The authors acknowledge the financial support of the project by the Economic Development and Innovation Operative Program of Hungary, GINOP-2.3.2-15-2016-00053: Development of liquid fuels having high hydrogen content in the molecule (contribution to sustainable mobility). The Project is supported by the European Union. Thanks are also due to the Interreg V-A Slovakia - Hungary Cooperation Program, SKHU/1902, (Project No: SKHU/1902/4.1/001) and to the Project (Project No. VEKOP-2.3.2-16-2017-00013) supported by the European Union and the State of Hungary, co-financed by the European Regional Development Fund. This work was also supported by the TKP2020-IKA-07 project financed under the 2020-4.1.1-TKP2020 Thematic Excellence Programme by the National Research, Development and Innovation Fund of Hungary.

Appendix A. Supplementary data

Supplementary data to this article can be found online at https://doi.org/10.1016/j.jcat.2021.08.052.

References

[1] G.W. Huber, S. Iborra, A. Corma, Synthesis of transportation fuels from biomass: Chemistry, catalysts, and engineering, Chem. Rev. 106 (2006) 4044–4098, https://doi.org/10.1021/cr068360d.
[2] L. Hermida, A.Z. Abdullah, A.R. Mohamed, Deoxygenation of fatty acid to produce diesel-like hydrocarbons: A review of process conditions, reaction kinetics and mechanism, Renew. Sustain. Energy Rev. 42 (2015) 1223–1233, https://doi.org/10.1016/j.rser.2014.10.099.
[3] K.A. Rogers, Y. Zheng, Selective deoxygenation of biomass-derived bio-oils within hydrogen-modest environments: A review and new insights, ChemSusChem 9 (2016) 1750–1772, https://doi.org/10.1002/cssc.201600144.
[4] M. Ameen, M.T. Azizan, S. Yusup, A. Ramli, M. Yasir, Catalytic hydrodeoxygenation of triglycerides: An approach to clean diesel fuel production, Renew. Sustain. Energy Rev. 80 (2017) 1072–1088, https://doi.org/10.1016/j.rser.2017.05.268.
[5] M. Anand, S.A. Farooqui, J. Singh, H. Singh, A.K. Sinha, Mechanistic in-operando FT-IR studies for hydroprocessing of triglycerides, Catal. Today 309 (2018) 11–17, https://doi.org/10.1016/j.cattod.2017.12.021.
[6] X. Li, X. Luo, Y. Jin, J. Li, H. Zhang, A. Zhang, J. Xie, Heterogeneous sulfur-free hydrodeoxygenation catalysts for selectively upgrading the renewable bio-oils to second generation biofuels, Renew. Sustain. Energy Rev. 82 (2018) 3762–3797, https://doi.org/10.1016/j.rser.2017.10.091.
[7] A. Sonthalia, N. Kumar, Hydroprocessed vegetable oil as a fuel for transportation sector: A review, J. Energy Inst. 92 (2019) 1–17, https://doi.org/10.1016/j.joei.2017.10.008.
[8] S. Khan, A.N. Kay Lup, K.M. Qureshi, F. Abnisa, W.M.A. Wan Daud, M.F.A. Patah, A review on deoxygenation of triglycerides for jet fuel range hydrocarbons, J. Anal. Appl. Pyrol. 140 (2019) 1–24, https://doi.org/10.1016/j.jaap.2019.03.005.

[9] P. Šimáček, D. Kubička, G. Šebor, M. Pospíšil, Hydroprocessed rapeseed oil as a source of hydrocarbon-based biodiesel, Fuel 88 (3) (2009) 456–460, https://doi.org/10.1016/j.fuel.2008.10.022.
[10] A.N. Kay Lup, F. Abnisa, W.M.A. Wan Daud, M.K. Aroua, A review on reactivity and stability of heterogeneous metal catalysts for deoxygenation of bio-oil model compounds, J. Ind. Eng. Chem. 56 (2017) 1–34, https://doi.org/10.1016/j.jiec.2017.06.049.
[11] L. Boda, G. Onyestyák, H. Solt, F. Lónyi, J. Valyon, A. Thernesz, Catalytic hydroconversion of tricaprylin and caprylic acid as model reaction for biofuel production from triglycerides, Appl. Catal. A 374 (1-2) (2010) 158–169, https://doi.org/10.1016/j.apcata.2009.12.005.
[12] S.D. Jackson, N.J. Casey, Hydrogenation of propyne over palladium catalysts, J. Chem. Soc., Faraday Trans. 91 (1995) 3269–3274, https://doi.org/10.1039/ft9959103269.
[13] G. Bergeret, P. Gallezot, Particle Size and Dispersion Measurements, in: G. Ertl, H. Knözinger, F. Schüth, J. Weitkamp (Eds.), Handb. Heterog. Catal., Wiley-VCH Verlag GmbH & Co. KGaA, Weinheim, Germany, 2008: pp. 738–765. 10.1002/9783527610044.hetcat0038.
[14] H. Knözinger, P. Ratnasamy, Catalytic aluminas: Surface models and characterization of surface sites, Catal. Rev. 17 (1978) 31–70, https://doi.org/10.1080/03602457808080878.
[15] G. Busca, V. Lorenzelli, V.S. Escribano, R. Guidetti, FT-IR study of the surface properties of the spinels $NiAl_2O_4$ and $CoAl_2O_4$ in relation to those of transitional aluminas, J. Catal. 131 (1991) 167–177, https://doi.org/10.1016/0021-9517(91)90333-Y.
[16] G. Busca, The surface of transitional aluminas: A critical review, Catal. Today 226 (2014) 2–13, https://doi.org/10.1016/j.cattod.2013.08.003.
[17] C. Morterra, G. Magnacca, A case study: Surface chemistry and surface structure of catalytic aluminas, as studied by vibrational spectroscopy of adsorbed species, Catal. Today 27 (1996) 497–532, https://doi.org/10.1016/0920-5861(95)00163-8.
[18] K. Khivantsev, N.R. Jaegers, J.-H. Kwak, J. Szanyi, L. Kovarik, Precise Identification and Characterization of Catalytically Active Sites on the Surface of γ-Alumina, Angew. Chemie Int. Ed. 60 (32) (2021) 17522–17530, https://doi.org/10.1002/anie.v60.3210.1002/anie.202102106.
[19] J.A.R. Van Veen, P.A.J.M. Hendriks, R.R. Andrea, E.J.G.M. Romers, A.E. Wilson, Chemistry of phosphomolybdate adsorption on alumina surfaces. 2. The molybdate/phosphated alumina and phosphomolybdate/alumina systems, J. Phys. Chem. 94 (13) (1990) 5282–5285, https://doi.org/10.1021/j100376a022.
[20] J.M. Lewis, R.A. Kydd, Adsorption mechanism of phosphoric acid on γ-alumina, J. Catal. 132 (1991) 465–471, https://doi.org/10.1016/0021-9517(91)90163-X.
[21] C. Morterra, G. Magnacca, P.P. Demaestri, Surface characterization of modified aluminas: III. Surface-features of PO_4-doped Al_2O_3, J. Catal. 152 (1995) 384–395, https://doi.org/10.1006/jcat.1995.1093.
[22] X. Wang, M. Shen, L. Song, Y. Su, J. Wang, Surface basicity on bulk modified phosphorus alumina through different synthesis methods, PCCP 13 (2011) 15589, https://doi.org/10.1039/c1cp21299k.
[23] E.C. DeCanio, J.C. Edwards, T.R. Scalzo, D.A. Storm, J.W. Bruno, FT-IR and solid-state NMR investigation of phosphorus promoted hydrotreating catalyst precursors, J. Catal. 132 (1991) 498–511, https://doi.org/10.1016/0021-9517(91)90166-2.
[24] C.A. Emeis, Determination of integrated molar extinction coefficients for infrared absorption bands of pyridine adsorbed on solid acid catalysts, J. Catal. 141 (2) (1993) 347–354, https://doi.org/10.1006/jcat.1993.1145.
[25] G. Busca, V. Lorenzelli, G. Ramis, R.J. Willey, Surface sites on spinel-type and corundum-type metal oxide powders, Langmuir 9 (6) (1993) 1492–1499, https://doi.org/10.1021/la00030a012.
[26] C. Morterra, G. Cerrato, C. Emanuel, End-on surface coordinated (adsorbed) CO_2: a specific ligand for surface Lewis acidic centres, Mater. Chem. Phys. 29 (1991) 447–456, https://doi.org/10.1016/0254-0584(91)90039-W.
[27] E.R.H. Van Eck, A.P.M. Kentgens, H. Kraus, R. Prins, A solid state double resonance NMR investigation of phosphorus-impregnated γ-Al_2O_3, J. Phys. Chem. 99 (1995) 16080–16086, https://doi.org/10.1021/j100043a057.
[28] J. Quartararo, M. Guelton, M. Rigole, J. Amoureux, C. Fernandez, J. Grimblot, Sol–gel synthesis of alumina modified by phosphorus: a solid state NMR characterization study, J. Mater. Chem. 9 (1999) 2637–2646, https://doi.org/10.1039/a903889b.
[29] J.S. Valente, S. Falcón, E. Lima, M.A. Vera, P. Bosch, E. López-Salinas, Phosphating alumina: A way to tailor its surface properties, Micropor. Mesopor. Mater. 94 (1-3) (2006) 277–282, https://doi.org/10.1016/j.micromeso.2006.02.018.
[30] J. Wang, Y. Wang, J. Wen, M. Shen, W. Wang, Effect of phosphorus introduction strategy on the surface texture and structure of modified alumina, Micropor. Mesopor. Mater. 121 (1-3) (2009) 208–218, https://doi.org/10.1016/j.micromeso.2009.01.035.
[31] J.A. Wang, X. Bokhimi, A. Morales, O. Novaro, T. López, R. Gómez, Aluminum local environment and defects in the crystalline structure of sol-gel alumina catalyst, J. Phys. Chem. B 103 (2) (1999) 299–303, https://doi.org/10.1021/jp983130r.
[32] M. Acikgoz, M.R. Khoshi, J. Harrell, A. Genova, R. Chawla, H. He, M. Pavanello, Tuning the electronic properties of the γ-Al_2O_3 surface by phosphorus doping, PCCP 21 (27) (2019) 15080–15088, https://doi.org/10.1039/C9CP03105G.
[33] N. Sheppard, T.T. Nguyen, The vibrational spectra of carbon monoxide chemisorbed on the surfaces of metal catalysts — a suggested scheme of interpretation., in: R.J.H. Clark, R.E. Hester (Eds.), Adv. Infrared Raman Spectrosc. Vol. 5, Heyden, London, 1978: p. 95.
[34] T. Lear, R. Marshall, J.A. Lopez-Sanchez, S.D. Jackson, T.M. Klapötke, M. Bäumer, G. Rupprechter, H.J. Freund, D. Lennon, The application of infrared spectroscopy to probe the surface morphology of alumina-supported palladium catalysts, J. Chem. Phys. 123 (2005), https://doi.org/10.1063/1.2101487 174706.
[35] T. Lear, R. Marshall, E.K. Gibson, T. Schütt, T.M. Klapötke, G. Rupprechter, H.-J. Freund, J.M. Winfield, D. Lennon, A model high surface area alumina-supported palladium catalyst, PCCP 7 (4) (2005) 565–567, https://doi.org/10.1039/B418708C.
[36] H.E. Evans, W.H. Weinberg, A comparison of the vibrational structures of ethanol, acetic acid, and acetaldehyde adsorbed on alumina, J. Chem. Phys. 71 (1979) 4789, https://doi.org/10.1063/1.438317.
[37] J. van den Brand, O. Blajiev, P.C.J. Beentjes, H. Terryn, J.H.W. de Wit, Interaction of anhydride and carboxylic acid compounds with aluminum oxide surfaces studied using infrared reflection absorption spectroscopy, Langmuir 20 (15) (2004) 6308–6317, https://doi.org/10.1021/la0496845.
[38] A.R. Barron, The interaction of carboxylic acids with aluminium oxides: Journeying from a basic understanding of alumina nanoparticles to water treatment for industrial and humanitarian applications, Dalton Trans. 43 (2014) 8127–8143, https://doi.org/10.1039/c4dt00504j.
[39] J.E. Tackett, FT-IR characterization of metal acetates in aqueous solution, Appl. Spectrosc. 43 (3) (1989) 483–489, https://doi.org/10.1366/0003702894202931.
[40] A.S. Milev, G.S.K. Kannangara, M.A. Wilson, Template-Directed Synthesis of Hydroxyapatite from a Lamellar Phosphonate Precursor, Langmuir 20 (5) (2004) 1888–1894, https://doi.org/10.1021/la0355601.
[41] K.D. Dobson, A.J. McQuillan, In situ infrared spectroscopic analysis of the adsorption of aliphatic carboxylic acids to TiO_2, ZrO_2, Al_2O_3, and Ta_2O_5 from aqueous solutions, Spectrochim. Acta - Part A: Mol. Biomol. Spectrosc. 55 (7-8) (1999) 1395–1405, https://doi.org/10.1016/S1386-1425(98)00303-5.
[42] Y. Ono, H. Hattori, Solid Base Catalysis, Springer, Berlin Heidelberg, Berlin, Heidelberg (2011), https://doi.org/10.1007/978-3-642-18339-3.
[43] E. Decanio, J.W. Bruno, V.P. Nero, J.C. Edwards, ^{27}Al NMR, FT-IR and Ethanol-^{18}O TPD Characterization of Fluorided Alumina, J. Catal. 140 (1) (1993) 84–102, https://doi.org/10.1006/jcat.1993.1070.
[44] G.A.H. Mekhemer, S.A. Halawy, M.A. Mohamed, M.I. Zaki, Ketonization of acetic acid vapour over polycrystalline magnesia: In situ Fourier transform infrared spectroscopy and kinetic studies, J. Catal. 230 (2005) 109–122, https://doi.org/10.1016/j.jcat.2004.09.030.